Physica B ■ (■■■■) ■■■–■■■

Contents lists available at ScienceDirect

Physica B

journal homepage: www.elsevier.com/locate/physb

Roles of doping ions in afterglow properties of blue $CaAl_2O_4:Eu^{2+},Nd^{3+}$ phosphors

A.H. Wako [a,*], B.F. Dejene [a], H.C. Swart [b]

[a] Department of Physics, University of the Free State, QwaQwa Campus, Private Bag X13, Phuthaditjhaba 9866, South Africa
[b] Department of Physics, University of the Free State, P.O. Box 339, Bloemfontein 9300, South Africa

ARTICLE INFO

Keywords:
$CaAl_2O_4:Eu^{2+}$
Nd^{3+}
Boric acid
Flux
Luminescence
Long afterglow

ABSTRACT

Eu^{2+} doped and Nd^{3+} co-doped calcium aluminate ($CaAl_2O_4:Eu^{2+},Nd^{3+}$) phosphor was prepared by a urea-nitrate solution combustion method at furnace temperatures as low as 500 °C. The produced $CaAl_2O_4:Eu^{2+},Nd^{3+}$ powder was investigated in terms of phase composition, morphology and luminescence by X-Ray diffraction (XRD), Scanning Electron Microscope (SEM), Fourier Transform Infra Red spectroscopy (FTIR) and Photoluminescence (PL) techniques respectively. XRD analysis depicts a dominant monoclinic phase that indicates no change in the crystalline structure of the phosphor with varying concentration of Eu^{2+} and Nd^{3+}. SEM results show agglomerates with non-uniform shapes and sizes with a number of irregular network structures having lots of voids and pores. The Energy Dispersive X-ray Spectroscopy (EDS) and (FTIR) spectra confirm the expected chemical components of the phosphor. PL measurements indicated one broadband excitation spectra from 200 to 300 nm centered around 240 nm corresponding to the crystal field splitting of the Eu^{2+} d-orbital and an emission spectrum in the blue region with a maximum on 440 nm. This is a strong indication that there was dominantly one luminescence center, Eu^{2+} which represents emission from transitions between the $4f^7$ ground state and the $4f^6$–$5d^1$ excited state configuration. High concentrations of Eu^{2+} and Nd^{3+} generally reduce both intensity and lifetime of the phosphor powders. The optimized content of Eu^{2+} is 1 mol% and for Nd^{3+} is 1 mol% for the obtained phosphors with excellent optical properties. The phosphor also emits visible light at around 587 and 616 nm. Such emissions can be ascribed to the $^5D_0$–$^7F_1$ and $^5D_0$–$^7F_2$ intrinsic transition of Eu^{3+} respectively. The decay characteristics exhibit a significant rise in initial intensity with increasing Eu^{2+} doping concentration while the decay time increased with Nd^{3+} co-doping. The observed afterglow can be ascribed to the generation of suitable traps due to the presence of the Nd^{3+} ions.

1. Introduction

The phenomenon of persistent luminescence refers to the ability of a material to absorb and store energy from light sources including visible and ultraviolet (UV) radiation, around it and to gradually release it as light at room temperature [1]. Persistent luminescent materials, which demonstrate an afterglow measured in hours, are of interest for various applications such as light emitting devices, fluorescent lamps, plasma display panels, lamps for medical applications, dark vision applications involving signage, intentional blackouts (deliberate power shutdown where electricity delivery is stopped for different parts of a region over periods of time for rationing purposes), emergency guidance systems and luminous watches among others. Persistent luminescence has been known since the early 1600s after the discovery of the Bologna stone [2], but the details of the storage and slow release of energy are still not fully explained. Rare earth (RE) co-doped calcium aluminate $CaAl_2O_4:Eu^{2+},Nd^{3+}$ forms part of a large group of alkaline earth aluminates $MAl_2O_4:Eu^{2+},R^{3+}$ (M=Ca, Sr, and Ba) [3] which are replacing the traditional ZnS:Cu,Co due to their persistent luminescence properties and also due to their chemical stability. They can easily be grown in crystalline form, and have a wide band gap of around 6 eV. Studies on the mechanism of persistent luminescence have focused on the interchange of the RE ions between the host band structure and the lattice defects.

The effect of Eu^{2+} ion (as a luminescence center) and Nd^{3+} concentration in the enhancement (or decrease) of the luminescence properties of $CaAl_2O_4:Eu^{2+},Nd^{3+}$co-doping has become field of interest. For long persistence materials, the depth and number of traps are critical factors in determining their performance. To achieve long persistence, RE ions are usually doped into hosts with complicated structures, because it is easier to form defect-related traps in such hosts. The ability of the RE species to

* Corresponding author. Tel.: +27 58 718 5264; fax: +27 58 718 5444.
E-mail addresses: wakoah@qwa.ufs.ac.za, alihwako@gmail.com (A.H. Wako).

0921-4526/$ - see front matter © 2013 Elsevier B.V. All rights reserved.
http://dx.doi.org/10.1016/j.physb.2013.11.023

trap electrons or holes can be determined from the location of the 4f and 5d levels of the Eu^{2+} and the Nd^{3+} ions in the band structure of the host [4], but the positions of these levels alone cannot offer enough explanation of the energy storage and luminescent mechanism [1] hence the role of lattice defects. In the present work, a systematic investigation was carried out on the Eu^{2+} doped $CaAl_2O_4$ phosphors. Especially the roles of Eu^{2+} and Nd^{3+} in persistent luminescence were discussed. Samples of $CaAl_2O_4$:Eu^{2+} and $CaAl_2O_4$:Eu^{2+},Nd^{3+} were synthesized by a solution combustion method in liquid phases so that the amount of each component can be accurately controlled and uniformly mixed. Compared with other conventional methods, the solution combustion process is very facile, safe, energy saving and only takes a few minutes. Analysis of the thermoluminescence (TL) glow curves is one of the most significant ways to measure the number of traps and also the activation energy of the trap levels in luminescent materials. TL properties of the $CaAl_2O_4$:Eu^{2+} and $CaAl_2O_4$:Eu^{2+},Nd^{3+} phosphors were investigated above room temperature by using a Nucleonix 1009I TL reader. The trap depths were estimated with the aid of the peak shape method.

2. Experimental

2.1. Synthesis

The polycrystalline Eu^{2+} doped and Nd^{3+} co-doped calcium aluminate, $CaAl_2O_4$:Eu^{2+} and $CaAl_2O_4$:Eu^{2+},Nd^{3+}, were prepared by a low temperature urea–nitrate solution combustion reaction between stoichiometric mixtures consisting of analytical pure grade $Ca(NO_3)\cdot 4H_2O$, $Al(NO_3)_3\cdot 9H_2O$, $Eu(NO_3)_2$, and $Nd(NO_3)_3$ as starting materials with urea, $CO(NH_2)_2$ as a fuel. Boric acid (H_3BO_3) was added as a flux to help enhance the photoluminescence. Two sets of samples containing 1:2 mol% ratios of $Ca(NO_3)\cdot 4H_2O$ and $Al(NO_3)_3\cdot 9H_2O$ were prepared. In order to investigate the effects of dopant (Eu^{2+}) and co-dopant (Nd^{3+}), the concentrations of Eu $(NO_3)_2$ and $Nd(NO_3)_3$ were gradually varied from 0.5 mol% and 0.25 mol% to 4 mol% moles respectively. In the first set only Eu $(NO_3)_2$ was added while the second set contained both $Eu(NO_3)_2$ and $Nd(NO_3)_3$ plus equal amounts of $CO(NH_2)_2$ as fuel. The masses were weighed and mixed with 10 ml of deionised water and

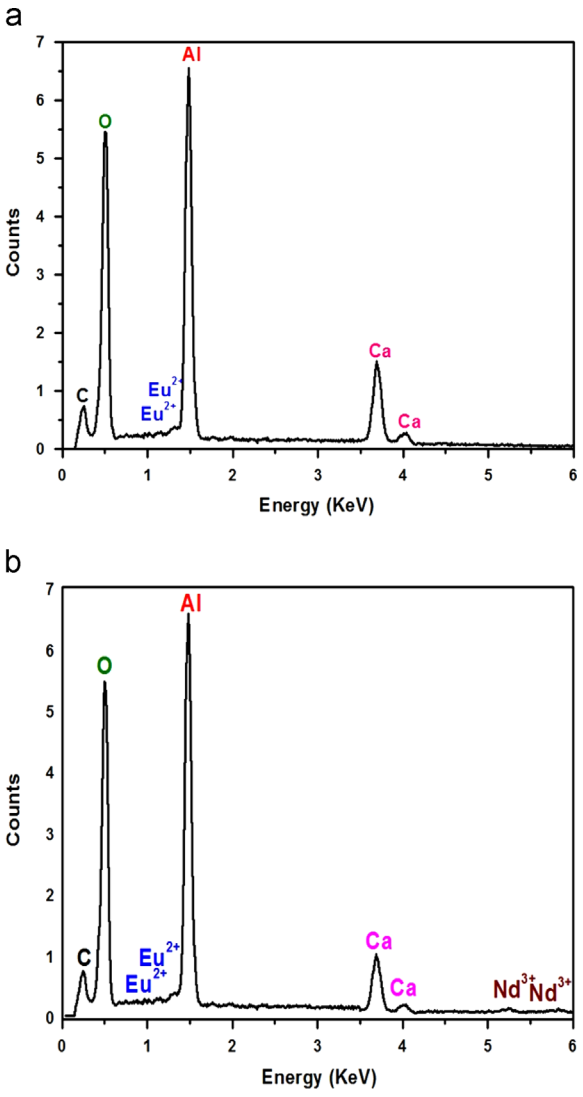

Fig. 2. EDS micrograph revealing the composition of the (a) $CaAl_2O_4$:3mol% Eu^{2+} and (b) $CaAl_2O_4$:3 mol% Eu^{2+}, 3 mol% Nd^{3+}.

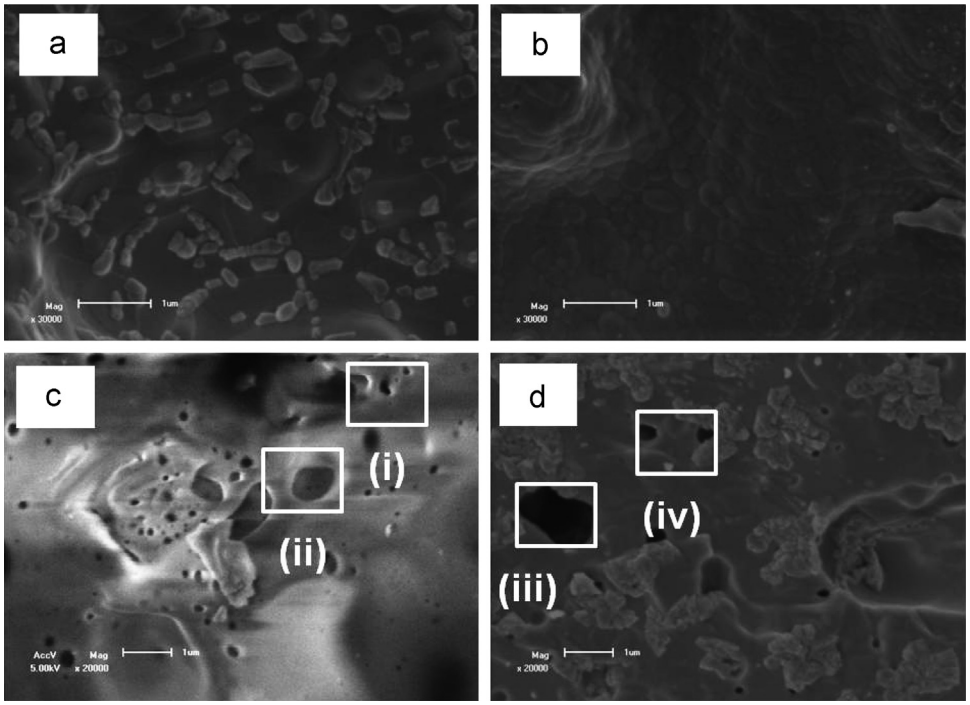

Fig. 1. SEM images of the microstructures for (a) 0.5 mol% Eu^{2+} (b) 1 mol% Eu^{2+}(c) 0.5 mol% $Nd^{3+}$and (d) 0.25 mol% Nd^{3+}.

stirred for 15 min at room temperature. The solutions were then poured into China crucibles and placed one at a time in a muffle furnace pre-heated at 500 °C. Initially, the solution started to boil and evaporation occurred followed by decomposition with release of fumes and gases (oxides of carbon, nitrogen and ammonia). Then, spontaneous ignition occurred and underwent a smoldering combustion with enormous swelling, producing white foamy and voluminous ash. The combustion ash was then milled to obtain the phosphor powders which were stored in glass sample bottles for characterization.

2.2. Characterization

The phase composition of the powders were determined by XRD using Philips model Bruker D8 Advance X-ray diffractometer with Cu Kα irradiation (λ=1.5406 Å) graphite target and monochromatized secondary, V=40 kV, A=40 mA Ni filter in the 2θ range from 20° to 80°. Scanning electron micrographs (SEM) used to study the morphology and particle size of the powder were taken using a Shimadzu model SSX-550 superscan Scanning Electron Microscope (SEM) equipped with Energy Dispersive x-ray spectrometer (EDS) to provide information about chemical composition of the material. Also to identify the products, Fourier transform infra red (FTIR) measurements were done using a Bruker Tensor 27 spectrometer. Emission spectra, excitation spectra, afterglow spectra and decay curve were measured at room temperature with a Cary Eclipse fluorescence spectrophotometer, model LS-55 with a built-in 150 W xenon flash lamp as the excitation source and a grating to select a suitable excitation wavelength. Thermoluminescence (TL) analyses were done above room temperature by using Nucleonix 1009I TL reader to investigate traps and defects in the solid $CaAl_2O_4$:Eu^{2+} and $CaAl_2O_4$:Eu^{2+},Nd^{3+} materials respectively.

3. Results and discussion

3.1. SEM and EDS analyses

Representative SEM micrographs for $CaAl_2O_4$:0.5 mol%Eu^{2+} and $CaAl_2O_4$:1 mol%Eu^{2+} phosphors are shown in Fig. 1(a) and (b) respectively. It can be observed that powders are in the form of agglomerates with non-uniform shapes and sizes caused by the

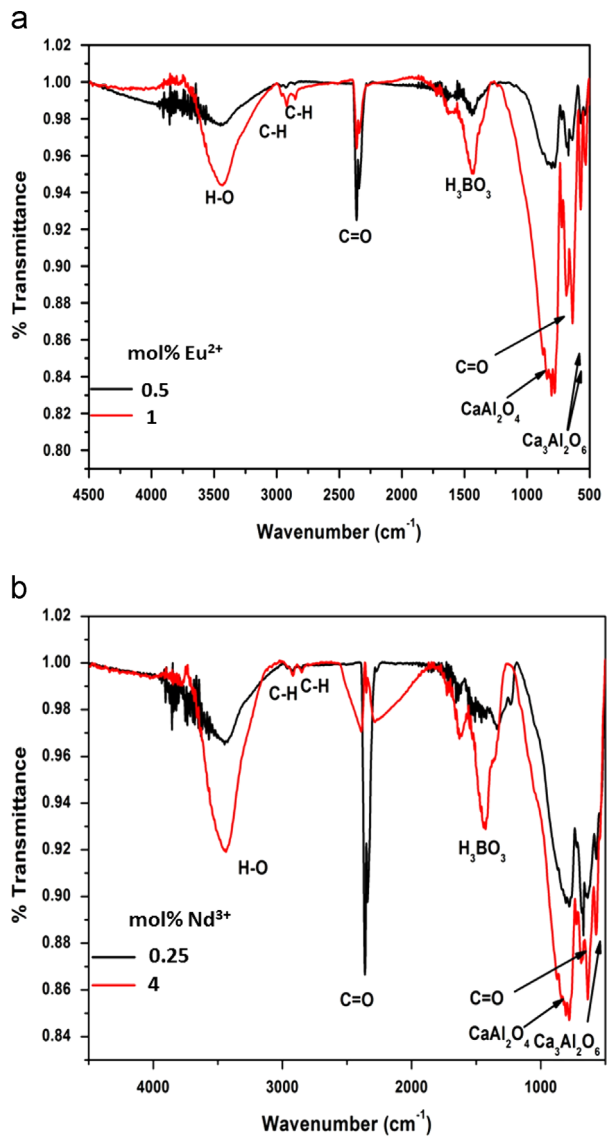

Fig. 3. (a) and (b) FTIR spectra for 0.5 mol% and 1 mol% Eu^{2+} and 0.25 mol% and 4 mol% Nd^{3+} respectively.

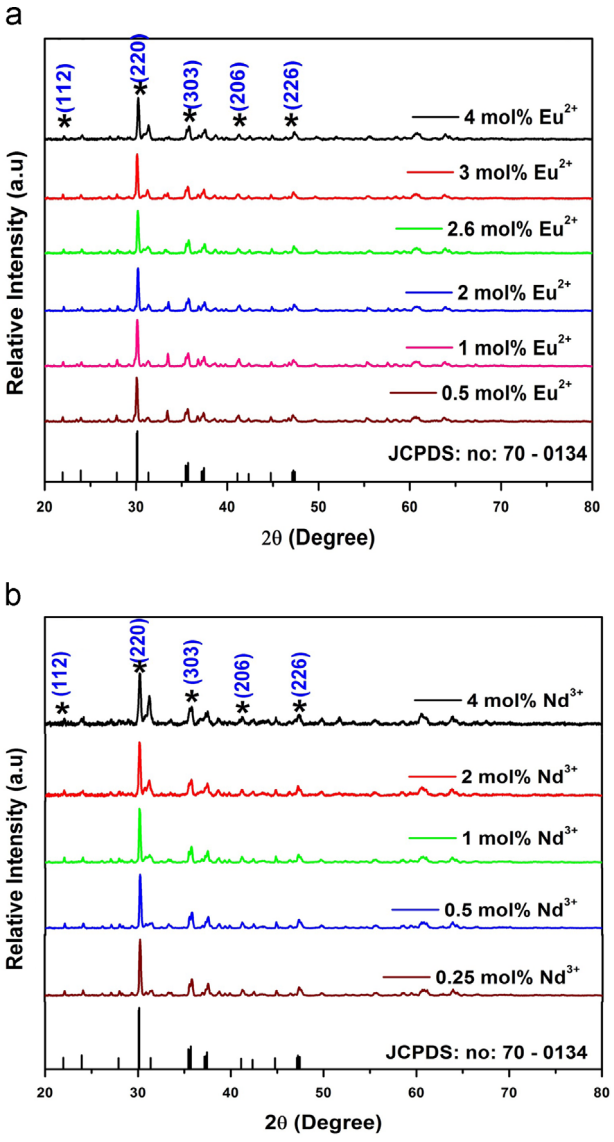

Fig. 4. Effects of the concentration of (a) Eu^{2+} and (b) Nd^{3+} on the structure of the $CaAl_2O_4$:Eu^{2+},Nd^{3+} phosphor.

non-uniform distribution of temperature and irregular mass flow during combustion. Fig. 1(c) and (d) shows the SEM results of $CaAl_2O_4$:1 mol%Eu^{2+}, 0.25 mol%Nd^{3+} and $CaAl_2O_4$:1 mol%Eu^{2+}, 0.5 mol%Nd^{3+} respectively. The plates contain a number of irregular network structures with lots of voids and pores formed by the escaping gaseous products during combustion of the nitrates as can be seen in Fig. 1(c) (zones (i) and (ii)) and (d) (zones (ii) and (iii)) respectively. The foamy microstructure of the aluminates reflects the inherent nature of the combustion process.

The EDS analysis was carried out to confirm the presence of Eu^{2+} and Nd^{3+} ions in the $CaAl_2O_4$:1 mol%Eu^{2+} and $CaAl_2O_4$:1 mol%Eu^{2+}, 1 mol%Nd^{3+} phosphors as shown in Fig. 2(a) and (b) respectively. The (EDS) spectra vary in intensities but confirm that the nano-phosphors are composed of aluminum (Al), calcium (Ca), oxygen (O), europium (Eu) and neodymium (Nd). The carbon tape used to support the sample during the analysis is responsible for the carbon peak (C) visible in the two profiles. Also, the effect of un-equivalent substitution is visible in Fig. 2. In crystals of $CaAl_2O_4$:Eu^{2+},Nd^{3+} the Ca^{2+} ion is the only metal ion that could be replaced by the Nd^{3+}, because there is such a great difference between the radii of Al^{3+} and Nd^{3+} that the replacement of Al^{3+} by Nd^{3+} is impossible. Therefore, besides Eu^{2+}, Nd^{3+} also replaces the sites of Ca^{2+} in crystals of Eu^{2+}, Nd^{3+} co-doped aluminate phosphors, which may explain the reduced Ca^{2+} intensity (counts) in Fig. 2 (b).

FTIR spectra of the samples are shown in Fig. 3(a) and (b). The characteristic of the molecule as a whole is reflected in the region from $\cong$1500 to 400 cm^{-1} known as the fingerprint region. Traces of $Ca_3Al_2O_6$ phase are detected in the in the region 420 to 680 cm^{-1} which are not captured in the XRD results since FTIR method, in many cases is more sensitive than XRD when determining presence of new phases [5,6], while the bands at 807 cm^{-1} are from CaA_2lO_4 signals [7]. The asymmetrical stretch of C═O signals which are due to CO_2 from the atmosphere gives a strong band at 2350 cm^{-1} and a degenerate peak appearing at 666 cm^{-1} in the IR spectrum. The signals at 1450 cm^{-1} show presence of H_3BO_3 while bands at 3450 cm^{-1} represent the vibration of water bonds [8]. From Fig. 3(b) we observe an increase in the absorbance intensity indicating that Nd^{3+} enhances absorption as compared to Eu^{2+} as shown in Fig. 3(a). The same is also reflected in the PL spectra of Figs. 5 and 6 respectively.

3.2. XRD analysis

X-ray diffraction measurements were employed to acquire information about the crystal structure of the doped $CaAl_2O_4$ powders. The XRD patterns of as-prepared Eu-doped host ($CaAl_2O_4$:Eu^{2+}) and when co-doped with Nd^{3+} ion ($CaAl_2O_4$:Eu^{2+},Nd^{3+}), are shown in Fig. 4(a) and (b) respectively. As can

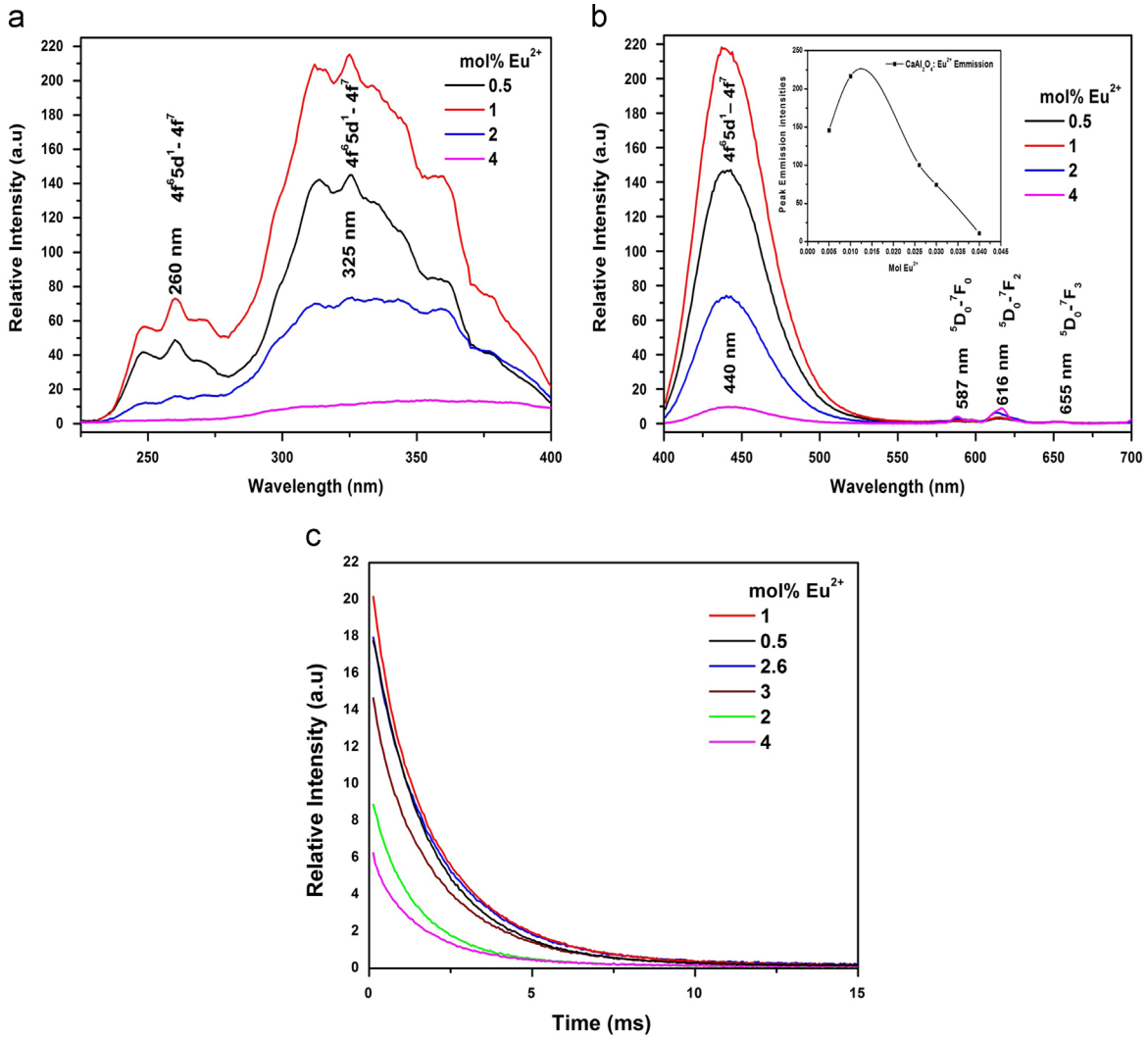

Fig. 5. (a) Excitation (λ_{em}=440 nm), (b) emission (λ_{ex}=325 nm) with inset for maximum peak emission intensities and (c) decay spectra of $CaAl_2O_4$:Eu^{2+} phosphor.

be seen, the monoclinic phase diffraction peaks of $CaAl_2O_4$ are predominant in the XRD patterns of the powders and all the major peaks could be indexed to the standard monoclinic $CaAl_2O_4$ (contrast JCPDS date File no. 70-0134). No other phase or unreacted starting material was observed except for the traces of $Ca_3Al_2O_6$ phase that were captured by the FTIR. This confirms the synthesized phase is dominantly low-temperature monoclinic phase (α-phase). In addition, the Eu^{2+} and Nd^{3+} dopants have no effect on the $CaAl_2O_4$ phase composition. This is in accordance with the reports [9].

3.3. Photoluminescence

3.3.1. Eu^{2+} doping

The excitation and emission spectra of $CaAl_2O_4$:Eu^{2+} with various concentrations of Eu^{2+} are shown in Fig. 5(a) and (b), respectively. Fig. 5(a) indicates that the excitation spectra of $CaAl_2O_4$:Eu^{2+} phosphor are similar to each other in shape, show a broad band from 280 to 400 nm and contain two excitation peaks; one main peak at 325 nm and a shoulder at 260 nm both due to $4f^65d^1$–$4f^7$ transition of Eu^{2+}. Fig. 5(b) illustrates that the emission spectra are all symmetrical about 440 nm which is attributed to the typical $4f^65d^1$–$4f^7$ transition of Eu^{2+} although the luminescent intensities vary greatly. It is also observed that high concentrations of Eu^{2+} generally reduce both intensity and lifetime of the phosphor powders. The results indicate that the luminescent intensity of $CaAl_2O_4$:Eu^{2+}, phosphor increased with Eu^{2+} concentration from 0.5 mol% to 1 mol% and drops with Eu^{2+} concentration in the range, 2–4 mol% Eu^{2+} respectively. This decrease in luminescence efficiency at higher dopant concentrations is due to the effect of concentration quenching [10]. The excitation at λ_{exc}=260 nm in Fig. 5(a) favours the Eu^{3+} emissions seen in the spectrum of Fig. 5(b). In Fig. 5(b), the peak at 587 nm is associated with $^5D_0$–$^7F_1$ transitions while the one located at 616 nm is due to the transitions from $^5D_0$–$^7F_2$ levels in Eu^{3+} respectively [11]. The peaks from $^5D_0$–$^7F_2$ (electric-dipole transition) is stronger than that from $^5D_0$–$^7F_1$ (magnetic-dipole transition), which indicates that the Eu^{3+} occupied the lattice sites without inversion symmetry in the $CaAl_2O_4$ host. The other peak at 655 nm is assigned to $^5D_0$–$^7F_3$ transitions. The presence of two kinds of transitions ΔJ=1(magnetic-dipole) and ΔJ=2 (electric-dipole) suggests at least two different crystallographic sites occupied by Eu^{3+} [12]. For long afterglow applications, the europium dopant has to be in its divalent state and this is supported by the high intensity of the $4f^65d^1$–$4f^7$ transition of Eu^{2+} in the $CaAl_2O_4$:Eu^{2+} phosphor as compared with the $^5D_0$–^7F_j (J=0, 1, 2,…,) of Eu^{3+} of Fig. 5(a) and (b), respectively. The relationship of the emission intensity with the amount of Eu^{2+} dopant is summarized in the inset of Fig. 5(b). It shows that 1 mol% Eu^{2+} gave the highest emission intensity.

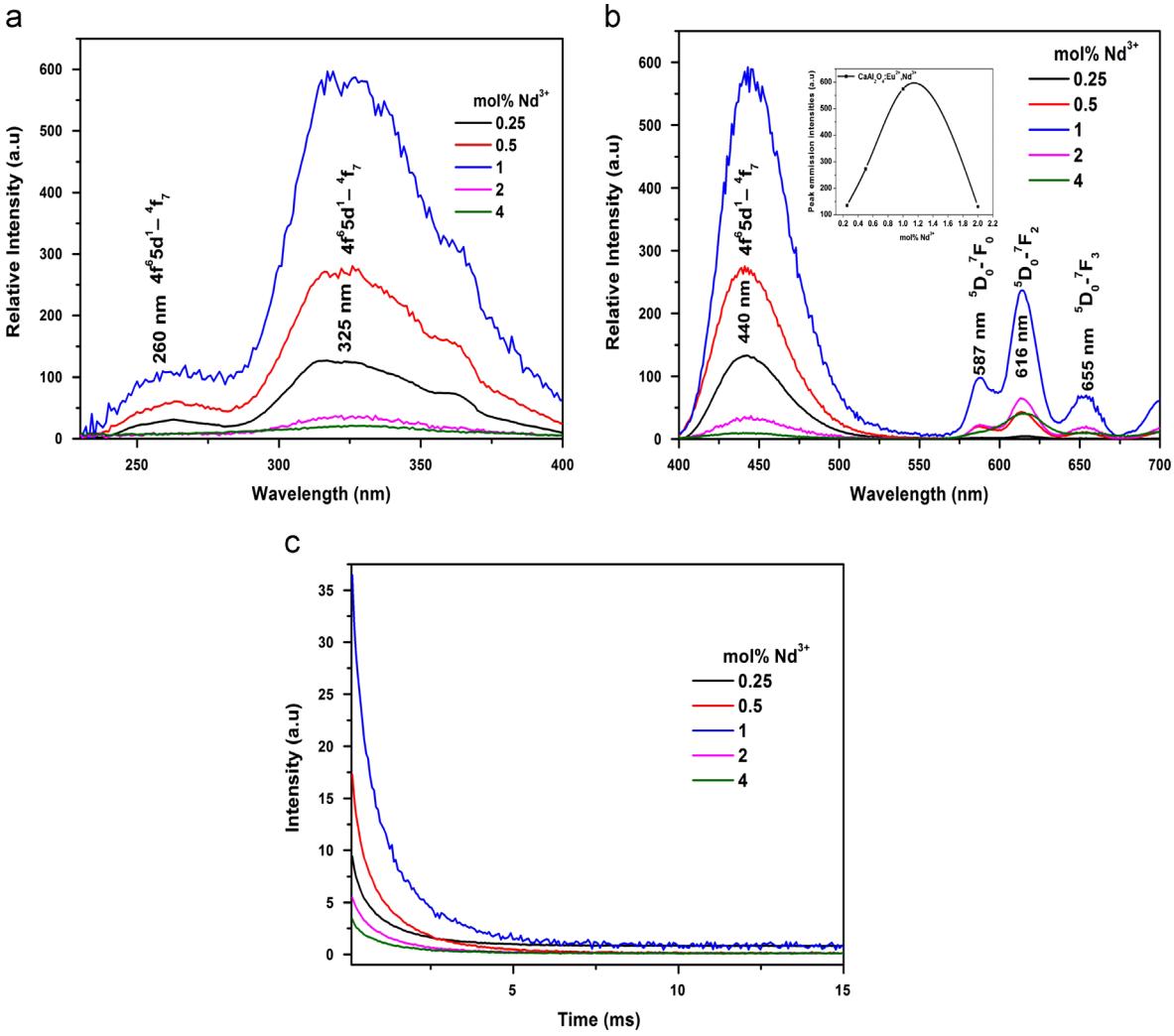

Fig. 6. (a) Excitation (λ_{em}=440 nm), (b) emission (λ_{ex}=325 nm) with inset for maximum peak emission intensities and (c) decay spectra of $CaAl_2O_4$:Eu^{2+},Nd^{3+} phosphor.

The luminescent decay curves of the $CaAl_2O_4$:Eu^{2+} phosphors doped with different moles of the divalent europium dopant (Eu^{2+}) at room temperature are showed in Fig. 5(c). It can be seen that the initial luminescence intensity and decay speed of afterglow of the phosphors are different from each other with 1 mol% Eu^{2+} still having the highest intensity in agreement with the other PL results.

3.3.2. Nd^{3+} co-doping

Similarly, Fig. 6(a–c) shows the PL spectra of the $CaAl_2O_4$:0.01Eu^{2+}, Nd^{3+} phosphor with various concentrations of Nd^{3+} as co-dopant. Compared with the $CaAl_2O_4$:0.01Eu^{2+} phosphor, $CaAl_2O_4$: 1 mol% Eu^{2+},Nd^{3+} exhibits a relatively higher luminescence intensity and a longer duration. This may be explained in two ways: firstly, the co-doped Nd^{3+} ions efficiently transferred the absorbed energy to the Eu^{2+} emitter. Secondly, the depth of traps formed by the co-doped Nd^{3+} ions was more suitable. In these figures, the PL intensity is observed to increase with an increase in Nd^{3+} concentration from 0.25 mol% to 1 mol% and decreased in the range 2–4 mol% of Nd^{3+}. This behavior can be attributed to concentration quenching effects [10]. The inset of Fig. 6(b) depicts variation of emission intensity with the amount of Nd^{3+} co-dopant.

It is suggested that long duration phosphorescence is dominated by the recombination process of the electrons, which were thermally released from the traps, with the Eu^{2+} as emitting centers [13]. Therefore, the afterglow characteristics of the $CaAl_2O_4$:1 mol%Eu^{2+},Nd^{3+} phosphor was affected greatly by the depth and the density of trap, which was formed by the Nd^{3+} ion co-dopant. This result is in good agreement with the TL glow curves in Fig. 7(b), which shows that the depth and density of traps do play a significant role in determining the afterglow characteristics of $CaAl_2O_4$:Eu^{2+},Nd^{3+} phosphor. The mechanism of the long persistence is due to the holes trapped–transported–de-trapped process [11]. Nd^{3+} ion works as traps of holes, and the trap levels lie in between the excited state and the ground state of the Eu^{2+} ions. After excited by the irradiation light, electron-and-hole pairs are produced in the Eu^{2+} ions, and the Nd^{3+} traps capture some of the free holes moving in the valence band. When the excitation source is cut off, some holes captured by the Nd^{3+} traps are thermally released slowly and relaxed to the excited state of Eu^{2+}, finally, returning to the ground state of Eu^{2+} accompanied with emission of visible light. This is the reason why a phosphor maintains a long persistent period of light emission after the excitation is stopped.

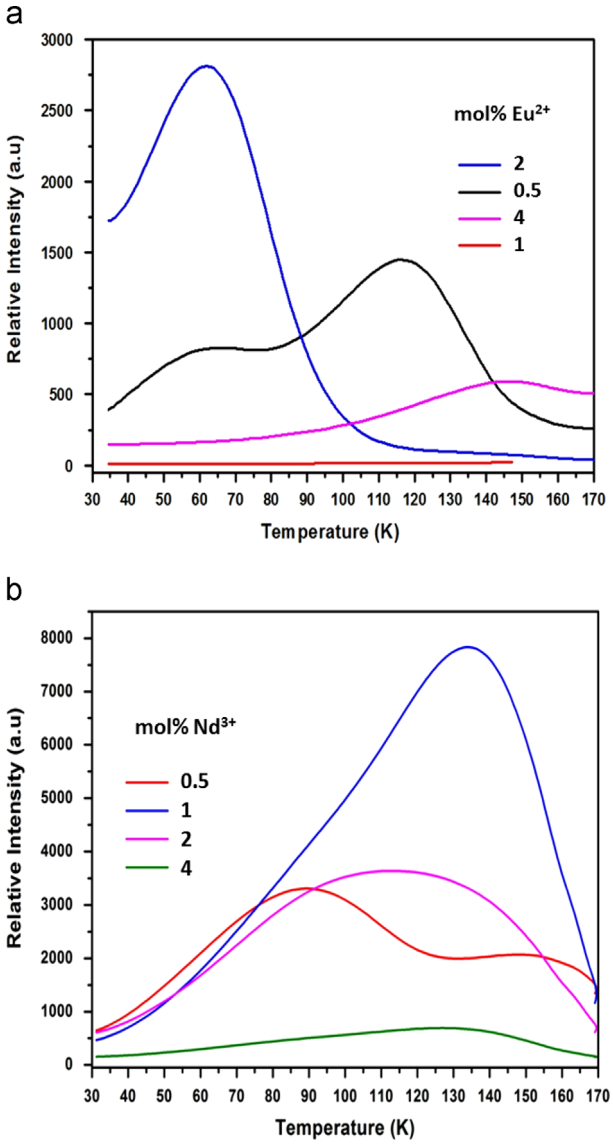

Fig. 7. (a) and (b) TL glow curves of $CaAl_2O_4$:Eu^{2+} as a function of mol Eu^{2+} and Nd^{3+} respectively.

4. Thermoluminescence

Thermoluminescence (TL) study is a useful method to reveal the trap depth and concentration of electron or hole traps in the crystal structure of a phosphor. The depth of the traps and their concentration in the phosphors can be obtained by analyzing the TL spectrum. The depth of each trap can be estimated from the peak temperature [14–16] using the equation

$$E = CY(KT_m^2/Y) - b_Y(2KT_m) \quad (1)$$

where T_m is the peak temperature, K is the Boltzmann constant, γ is chosen as the full width (temperature) of the peak at its half-height ($\gamma = T_2 - T_1$, where T_2 and T_1 are the temperatures at half peak height), and c_γ and b_γ are peak shape constants. It follows from the formula that the higher the peak temperature the deeper the trap depth. After co-doping $CaAl_2O_4$:1 mol%Eu^{2+} with 1 mol% Nd^{3+} ($CaAl_2O_4$:1 mol%Eu^{2+},1 mol%Nd^{3+}), it was found not only to have increased the intensity but also gave a new thermal peak which appeared at 135 K as depicted in Fig. 7(b), which definitely corresponds to the electron trap of Nd^{3+}. It was suggested that a suitable trap depth and a certain amount of concentration of the traps are essential for phosphors to show long persistence [17]. The trap was formed by the co-doped Nd^{3+} that replaces the original Ca^{2+} ion in the host lattice. A deeper trap level and a higher trap density will normally lead to a higher initial afterglow and longer persistence. The TL spectra further verified that Nd^{3+} co-doping would result in the creation of a new electron trap and can effectively enhance the persistent luminescence and thermoluminescence of the phosphor. This also corresponds with the results obtained under PL analysis in this study.

5. Conclusion

In this work we obtained crystalline $CaAl_2O_4$:1 mol%Eu^{2+} and $CaAl_2O_4$:1 mol%Eu^{2+},1 mol%Nd^{3+} powders at relatively low temperature by the solution-combustion method. The influences of the varying quantities of Eu^{2+} and Nd^{3+} on the properties of the phosphor were studied. The analytical results indicate that the broad emitted band of the $CaAl_2O_4$:1 mol%Eu^{2+},1 mol%Nd^{3+} is

observed in the blue region (λ_{max}=440 nm) due to transitions from the $4f^6 5d^1$–$4f^7$ configuration of the Eu^{2+} ion. The (TL) glow curves of $CaAl_2O_4$:1 mol%Eu^{2+} phosphor revealed an afterglow when co-doped with Nd^{3+} ion, which can be ascribed to the different traps formed by the Nd^{3+} ion within the $CaAl_2O_4$ host. (SEM) observations showed that powders are in the form of agglomerates with irregular shapes and sizes caused by the non-uniform distribution of temperature and irregular mass flow during combustion. Also, irregular network structures with lots of voids and pores formed by the escaping gaseous products during combustion of the nitrates were observed.

Acknowledgments

Financial support from the National Research Foundation (NRF) of the government of South Africa and the services of the research equipment of University of Free State, Physics department used in this study are gratefully acknowledged by the authors.

References

[1] T. Aitasalo, J. Hölsä, H. Jungner, M. Lastusaari, J. Niittykoski, J. Phys. Chem. B 110 (2006) 4589.
[2] E. Harvey, A History of Luminescence: From the Earliest Times Until 1900.
[3] B. Mothudi, O. Ntwaeaborwa, J. Botha, H. Swart, Physica B: Phys.Condens. Matter 404 (22) (2009) 4440.
[4] T. Matsuzawa, Y. Aoki, N. Takeuchi, Y. Murayama, J. Electrochem. Soc. 143 (1996) 2670.
[5] C.M. Phillippi, K.S. Mazdiyasni, J. Am. Ceram. Soc. 54 (1971) 254.
[6] T. Hirata, E. Asari, M. Kitajima, J. Solid State Chem. 110 (1994) 201.
[7] L. Fernández-Carrasco, D. Torrens-Martín, L.M. Morales, S. Martínez-Ramírez, Infrared Spectroscopy in the Analysis of Building and Construction Materials, ISBN: 978-953-51-0537-4, 2012, p. 370.
[8] F. Miller, C. Wilkins, Anal. Chem. 24 (8) (1952) 1253.
[9] H. Ryu1, K.S. Bartwal, Res. Lett. Mater. Sci. 1155 (2007) 23643.
[10] D. Fumo, M. Morelli, A. Segadães, Mater. Res. Bull. 31 (1996) 1243.
[11] C. Ronda, Luminescence - From Theory to Applications, Wiley-VCH; Weinheim (2008) 8.
[12] S. Janáková, L. Salavcova, G. Renaudin, Y. Filinchuk, D. Boyer, P. Boutinaud, J. Phys. Chem. Solids 68 (5–6) (2007) 1147.
[13] Y. Lin, Z. Zhang, Z. Tang, J. Zhang, Z. Zheng, X. Lu, Mater. Chem. Phys. 70 (2001) 156.
[14] S. McKeever, Thermoluminescence of Solids, Cambridge University Press (1985) 88.
[15] T. Kim, J. Woo, H. Choe, H. Kang, H. Jang, C. Whang, Radiat. Prot. Dosim. 84 (1) (1999) 297.
[16] Q. Su, Rare-Earth Chemistry, Science and Technology Press, Zhenzhou (1993) 13.
[17] M. Jahan, D. Cooke, W. Hults, J. Lumin. 47 (1990) 85.